



City Research Online

City, University of London Institutional Repository

Citation: Song, J., Ghosh, S., Zhang, H., Zhou, L. & Rahman, B. M. (2019). Design, optimization, and performance evaluation of GSST clad low-loss non-volatile switches. *Applied Optics*, 58(31), pp. 8687-8694. doi: 10.1364/ao.58.008687

This is the accepted version of the paper.

This version of the publication may differ from the final published version.

Permanent repository link: <https://openaccess.city.ac.uk/id/eprint/23157/>

Link to published version: <https://doi.org/10.1364/ao.58.008687>

Copyright: City Research Online aims to make research outputs of City, University of London available to a wider audience. Copyright and Moral Rights remain with the author(s) and/or copyright holders. URLs from City Research Online may be freely distributed and linked to.

Reuse: Copies of full items can be used for personal research or study, educational, or not-for-profit purposes without prior permission or charge. Provided that the authors, title and full bibliographic details are credited, a hyperlink and/or URL is given for the original metadata page and the content is not changed in any way.

City Research Online:

<http://openaccess.city.ac.uk/>

publications@city.ac.uk

Design, Optimisation and Performance evaluation of GSST clad low-loss non-volatile switches

JUNCHAO SONG, ^{1,*} SOUVIK GHOSH, ¹ HANYU ZHANG, ² LINJIE ZHOU, ² AND B. M. A. RAHMAN, ¹

¹Department of Electrical and Electronic Engineering, School of Engineering, City, University of London, London, EC1V 0HB, U.K.

²State Key Laboratory of Advanced Optical Communication Systems and Networks, Department of Electronic Engineering, Shanghai Jiao Tong University, Shanghai 200240, China.

* Junchao.Song@city.ac.uk

Abstract

In this paper, we investigate performance of a self-sustained ON-OFF switch incorporating a new phase change material $\text{Ge}_2\text{Sb}_2\text{Se}_4\text{Te}_1$ with Silicon rib waveguide at the telecommunication wavelength $1.55 \mu\text{m}$. A full-vectorial \mathbf{H} -field finite element method is used to find effective index and modal loss of the quasi-TE modes in GSST-Si waveguide. Both the electro-refraction and electro-absorption type design are studied and the effect of GSST thickness and Si slab thickness on the device performances are presented. These results suggest that a GSST-Si rib waveguide with a 500 nm wide Si core, $60\text{-}90 \text{ nm}$ Si slab thickness, and $40\text{-}60 \text{ nm}$ GSST layer could be a realistic switch design which can yield a very compact, $5 \mu\text{m}$ long device with only 0.135 dB total insertion loss and more than 20 dB extinction ratio.

© 2019 Optical Society of America under the terms of the [OSA Open Access Publishing Agreement](#)

1. Introduction

It is important to reducing the size of active photonic devices, such as optical switches and modulators to increase the integration density of photonic integrated circuit (PIC). Over the past decades, photonic devices based on Si-on-insulator (SOI) platform are showing promise due to reduced PIC's footprint and power consumption and also for their compatibility with microelectronic circuits based on CMOS technology.

One of the most common method of achieving modulation in Si devices so far has been to utilize the plasma dispersion effect. This effect can be achieved through carrier injection or depletion by electrical manipulation of the free-carrier density interacting with the propagating light [1]. In the first case, carriers are injected through forward biasing the junction which provide a high modulation depth but limited by the slow recombination rate of the carriers and consumes relatively high power. For carrier depletion, carrier density is modulated by reverse biasing junction, which is relatively fast and consumes less power but suffer from a larger insertion loss due to the initial doping of PN junction and also lower modulation efficiency due to the small change in the depletion width.

The phase change material (PCM), exhibits a large difference in both real and imaginary parts of its refractive index when undergoing a solid-state transition and can be used to solve some of these problems caused by the plasma dispersion effect devices [2]. Recently, the scope for PCM has been expanded to oxides, such as vanadium dioxide (VO_2). Although VO_2 has a large refractive index change during its phase transition, however the associated losses in both phases are high which makes the device volatile and also require continuous power to maintain each state [3]. Another phase change material $\text{Ge}_2\text{Sb}_2\text{Te}_5$ (GST) has been reported with better

optical performance than the VO₂ [4] [5]. The high refractive index changes between the amorphous and crystalline states of GST is exploited to yield a more compact switch. The phase change of the GST can be thermally [6], optically [7], or electrically [8] induced and thus can potentially operate at an ultrahigh speed. Besides that, GST possesses the self-holding feature, unlike other electro-optic materials, which means it only requires energy to switch from one state to another, and continuous supply of energy is not required to maintain a given state. Despite these attractive features, GST still suffer from excessive optical losses even in the amorphous state due to its small bandgap and the resulting interband absorption in the telecommunication bands. For instance, the imaginary part of GST amorphous refractive index is 0.04 at 1550 nm wavelength, corresponding to 14000 dB/cm attenuation, which fundamentally limits many applications [9].

A new, low-loss optical phase change material has recently been reported which can overcome the limitations of GST based optical switching devices [10]. The Ge₂Sb₂Se₄Te₁ (GSST), derived in GST by partially substituting Te with Se, which increases the optical bandgap, enabling reduced loss in the 1310 nm and 1550 nm telecommunication bands. The complex refractive index of GSST at operating wavelength 1550 nm, measured by ellipsometer on thermally evaporated films, are taken as n (Amorphous-GSST) = 3.4 + j 0.00018, n (Crystalline-GSST) = 5.1 + j 0.5, respectively [10]. The large index contrast between the amorphous and crystalline states and the low optical extinction coefficient of GSST amorphous state, which is only 0.00018, over 200 times smaller than that of the GST and thus showing considerable promise to integrated with SOI platform for the low-loss, non-volatile switching photonic devices design.

In this paper, the design optimization of a compact ON-OFF switch based on a GSST-Si rib waveguide is proposed at the telecommunication wavelength 1.55 μ m. Here, a rigorous **H**-field based full-vectorial finite-element method (VFEM) in conjunction with the perturbation technique is used to find the complex modal propagation constant with the variations of the waveguide parameters. Following that, the least squares boundary residual (LSBR) method, is used to calculate the coupling loss at the butt-coupled junctions to identify the best waveguide parameters to achieve a lower insertion loss and a higher extinction ratio. Following that, the proposed design is also validated by the Finite Difference Time-Domain (FDTD) simulations.

2. Theory and design method

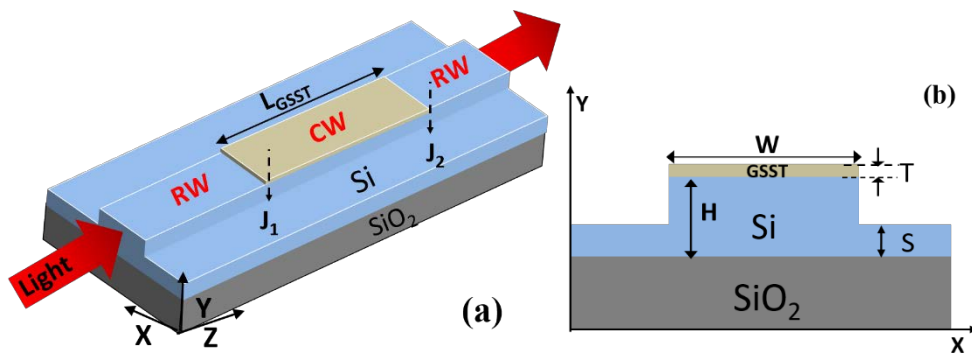


Fig. 1. (a) Schematic of the GSST-Si optical switch, (b) Cross-sectional view of the coupled section CW.

The three-dimensional view of the self-sustained optical switch based on the GSST-Si rib waveguide, identified here as CW is shown in Fig. 1(a). Here, outer two unclad rib waveguide

sections are passive, also identified as RW, while the middle CW section is active. The active section consists of a standard single-mode Si rib waveguide with GSST deposited on the top. A rib waveguide is considered over a fully etched nanowire waveguide. From the waveguide fabrication point, it is often difficult to maintain the surface smoothness of the completely etched vertical sidewalls. This surface roughness introduces scattering loss which is not preferable for the integrated optical switching applications. Compare to the ridge waveguide, a rib waveguide is easy to fabricate and less prone to show the scattering loss due to its partially etched side walls. Therefore, in our design, we preferred a rib waveguide for the GSST-based switching application. The cross-sectional view of the CW section is shown in Fig. 1(b). Here, thickness of the Si core is identified as H and kept constant at 220 nm, its width identified as W, also kept constant at 500 nm, and the slab layer thickness shown as S, is varied. The length of GSST clad for optical switching, is taken as L_{GSST} .

2.1 Modal analysis method

The eigenmodes of all practical optical waveguides with 2-D confinement are quasi-TE and quasi-TM modes, with all the three components of both \mathbf{E} and \mathbf{H} fields. The full-vectorial \mathbf{H} -field based finite element method, one of the most accurate and numerically efficient approaches, is used here for the modal analyses [11]. The variational formulation using the vectorial \mathbf{H} -field with the penalty term can be given as:

$$\omega^2 = \frac{\int [(\nabla \times \mathbf{H})^* \cdot \varepsilon^{-1} \cdot (\nabla \times \mathbf{H}) dx dy + \rho (\nabla \times \mathbf{H})^* \cdot (\nabla \times \mathbf{H})] dx dy}{\int \mathbf{H}^* \cdot \mu \cdot \mathbf{H} dx dy} \quad (1)$$

where, \mathbf{H} is the full-vectorial magnetic field, * denotes a complex conjugate and transpose, ω^2 is the eigenvalue, ω is the angular frequency of the wave, ε and μ are the permittivity and permeability, respectively, and ρ is a weighting factor for the penalty term.

As the CW contain a layer of GSST cap with complex refractive index, it incurs modal loss. In this case, a full-vectorial \mathbf{H} -field finite element method incorporating the perturbation technique [12] would be more suitable to calculate the modal loss values for such waveguides with small modal loss used here.

2.2 Calculation of junction loss at the Si and Si-GSST waveguide interfaces.

When GSST layer is deposited on the top of the Si rib waveguide, the mode profile the guided mode is modified and this introduces insertion loss at these junctions. A lower coupling loss at the butt-coupled junctions for both the GSST states is desirable. The LSBR, a rigorous method is utilized to calculate the coupling loss between the input Si RW and the active GSST CW. To carry out these analyses, a full-vectorial FEM is used to find the modal field profiles of the cross-section at both sides of a discontinuity interface. Then, the LSBR method is used to calculate the power transfer efficiency by enforcing the required continuity of the tangential \mathbf{E} and \mathbf{H} fields at the junction interface to obtain the transmission and reflection coefficients of the fully hybrid modes at the discontinuity interfaces. The LSBR method looks for a stationary solution by minimizing the error energy functional J, to satisfy the continuity conditions of the tangential \mathbf{E} and \mathbf{H} fields in a least squares sense over the interface, as given by [13]:

$$J = \int |E_t^1 - E_t^2|^2 + \sigma \cdot z_0^2 |H_t^1 - H_t^2|^2 d\Omega \quad (2)$$

Where Z_0 is the free-space wave impedance and σ is the dimensionless weighting factor to balance the electric and magnetic components of the error functional. Here, 1 and 2 superscripts are used to identify fields in sides 1 and 2, respectively. The integration is carried out over the two junction interfaces, Ω , between the input Si RW and GSST CW shown by J_1 , and also GSST CW and output Si RW, shown by J_2 in Fig. 1.

3. Numerical results

3.1 Fundamental mode field profile

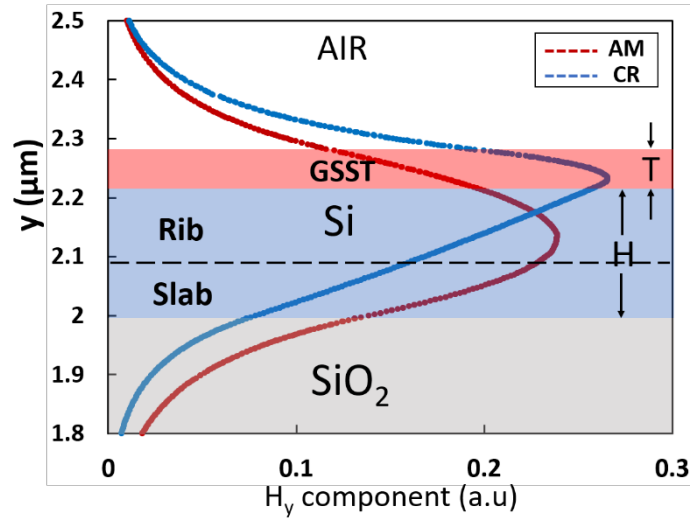


Fig. 2. H_y variation along the vertical direction, for GSST-Si CW in amorphous and crystalline state with $W=500$ nm, $H=220$ nm, $S=90$ nm, and $T=60$ nm.

We have used our in-house FEM codes [11] to obtain the modal solutions of the GSST CW. For the quasi-TE mode, H_y is the dominant component of the magnetic field, \mathbf{H} . The CW in amorphous state with $W = 500$ nm, $S = 90$ nm, $T = 60$ nm is simulated, and variation of the dominant H_y field of the quasi-TE H_y^{11} modes along the y -axis is shown in Fig. 2 by a red line. The SiO_2 buffer region is shown by a lower grey shade and Si region with a light blue shade and a dashed line inside identifies the interface between the slab and rib layers. The GSST layer is also shown by a red shade above the Si region. It can be noted that, when GSST in amorphous state, the field is mostly confined in the Si rib core and the maximum H_y value is inside the rib and near to the interface between the Si rib and slab.

The H_y field profile for an unclad waveguide RW is not shown here, but this was very similar as that of GSST in amorphous state. However, the GSST refractive index is increased considerably when it is switched to a crystalline state, significantly changing the mode field profile. Variation of H_y field of the H_y^{11} mode of CW in crystalline state along the y -axis is also shown in Fig. 2 by a blue line. It can be observed that the field is still confined well inside the Si rib core, but a large modal field is presented in the top GSST region. The maximum H_y value is rather inside the top GSST layer and just above the interface between the Si rib and the top GSST layer. It suggests that if the GSST is transformed to crystalline state, more power is absorbed into the GSST layer. The H_y field decays exponentially both in the upper air and lower SiO_2 regions.

3.2 Modal solution characteristics

For the modal solution, when the GSST is in amorphous state, the effective index of CW is written as $(n_{e1} + j^*k_{e1})$, and while in crystalline state, it can be written as $(n_{e2} + j^*k_{e2})$. The mode absorption loss α of the waveguide in dB per micrometer, can be calculated for each state from the imaginary part of their effective indices k_e , as

$$\alpha = 2 \times 10 \log e \times \left(\frac{2\pi k_e}{\lambda} \right) \quad (3)$$

Table 1. Modal solution characteristics

	n_e	k_e	Mode loss α (dB/ μm)
Amorphous	2.5723	6.8×10^{-4}	0.00024
Crystalline	2.6773	0.0415	1.46122
Difference	0.105	0.041493	1.46098

The calculated modal solution parameters for the H_y^{11} mode of CW ($W = 500$ nm, $S = 90$ nm, $T = 20$ nm) are given in Table 1. It can be noted that when GSST is in crystalline state, the waveguide has a larger effective index, both in real and imaginary parts, which also suggests a larger mode loss. Although these values depend on the waveguide design, but for a comparable design both these values are lower than the GST based design [14] along with a very low modal loss for the amorphous state.

An optical switch can be designed by exploiting either Electro-refraction (ER) or Electro-absorption (EA). Electro-refraction, which unitizes the differential of the real part of the effective index, is widely used to design optical switches. The ER based optical switch can be comprised of Mach-Zehnder interferometer (MZI) with two branches. For a MZ-based switch, a larger ER value is preferred for a compact device but also requires lower loss values for both the states. The CW considered here has a strong electro-refraction $ER = (n_{e2} - n_{e1}) = 0.105$, and a very low mode loss only 2.4×10^{-4} dB/ μm and may be suitable for the MZI design. On the other hand, the Electro-absorption effect can also be used for modulation, where the differential mode loss between the two states is exploited to achieve the optical switching. The CW here also has a strong electro-absorption $EA = (k_{e2} - k_{e1}) = 0.0415$, because it goes through significant change in the imaginary parts of GSST refractive indices induced by the phase change, which makes it possible to achieve a higher extinction ratio switching.

In the next section, variations of both ER and EA characteristics of the GSST-Si CW waveguide with its width and height of different layers are thoroughly investigated.

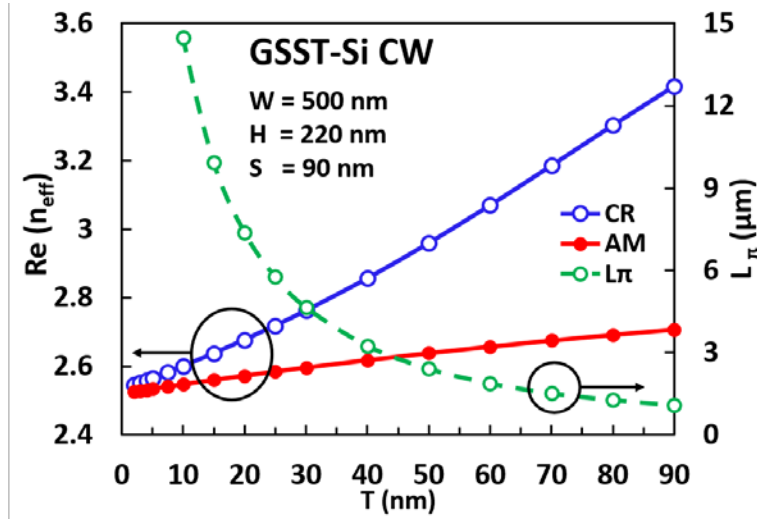


Fig. 3. Variations of the real part of effective indices for amorphous and crystalline states also L_{π} with the GSST thickness, T for CW.

Variations of real part of the effective index with the GSST layer thickness, T , are shown in Fig. 3, when $W = 500$ nm, $H = 220$ nm, and $S = 90$ nm. Results for amorphous state (AM) are shown by a red line with solid circles and those for the crystalline state (CR) are shown by a blue line with hollow circles. When GSST is in amorphous state, it can be observed that the n_{e1} increases with T as the deposited GSST layer with higher refractive index increases. On the other hand, the real part of the effective index for the crystalline state n_{e2} , also increases with T , but at a much higher rate than the amorphous state's values. This is because, when the GSST is in crystalline state, its refractive index is 1.5 times larger than that of the amorphous state so that the CW will have a higher effective index value for the crystalline state.

In switches, the phase change $\Delta\phi$ is the product of the differential propagation constant $\Delta\beta$ and the device length L , which affects the transfer of light from the input guide to the output guide. Here, $\Delta\phi$ is given as:

$$\Delta\phi = \Delta\beta L = \left(\frac{2\pi}{\lambda}\right) \cdot \Delta n_e \cdot L = \left(\frac{2\pi}{\lambda}\right) \cdot (n_{e2} - n_{e1}) \cdot L \quad (4)$$

For a Mach-Zehnder interferometer (MZI) based design, the value of " $\Delta\phi$ " needs to be equal to π rad, and the length L_{π} of such switches is calculated as:

$$L_{\pi} = \frac{\pi}{\Delta\beta} = \frac{\lambda}{2 \cdot \Delta n_e} = \frac{\lambda}{2 \cdot (n_{e2} - n_{e1})} \quad (5)$$

The L_{π} of the CW decrease gradually from 16 to 1.5 μm , as the difference between n_{e1} and n_{e2} increases with the GSST thickness, T , shown in Fig. 3 by a dashed green line using the right-hand side scale.

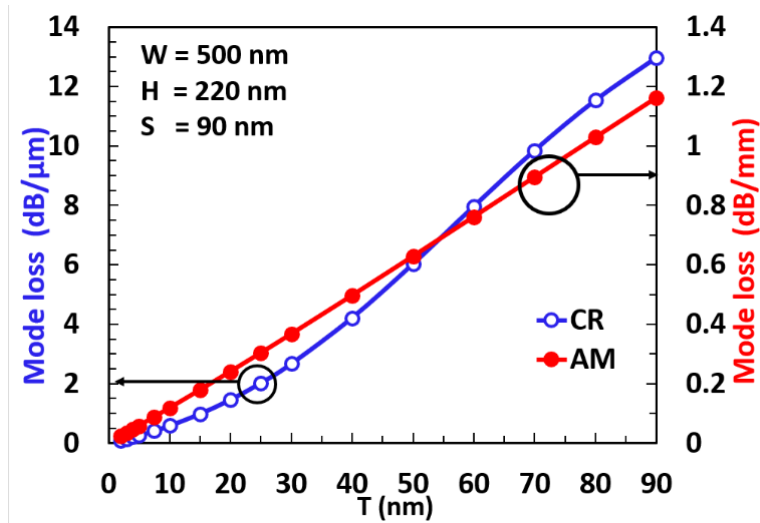


Fig. 4. Variations of mode loss of CW in amorphous and crystalline states with GSST thickness, T.

As GSST incurs material loss, so the variations of modal loss for these two states with the GSST thickness T are shown in Fig. 4. Results for the amorphous state (AM) are shown by a red line with solid circles, by using the right-hand side scale, while those for the crystalline state (CR) are shown by a blue line using the left-hand side scale incorporating hollow circles. When GSST is in amorphous state, it can be observed that the mode loss increases with T, as the top loaded GSST layer area increases. On the other hand, the mode loss for the crystalline state also increases with T, but these values are nearly four orders of magnitude larger than those in the amorphous state. This is because, for the GSST in the crystalline state, imaginary part of its refractive index is much larger than that in the amorphous state. When the T reduces to lower than 10 nm, the mode loss of CW for both the states will be relatively lower.

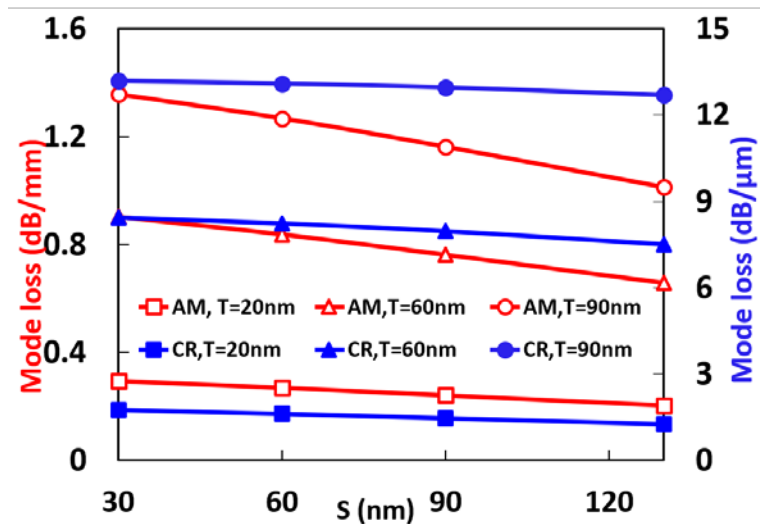


Fig. 5. Variations of mode loss of CW in amorphous and crystalline states with Si slab thickness, S of three different values of T (W = 500 nm, H = 220 nm).

Next, variations of modal loss with the Si slab thickness for different GSST thickness T in these two states are shown in Fig. 5. Results for the amorphous state (AM) are shown by red lines with hollow circles, using the left-hand side scale, while those for the crystalline state (CR) are shown by blue lines with solid circles using the right-hand side scale. When GSST is in amorphous state, it can be observed that all the GSST thickness waveguide mode loss values decrease when the slab thickness S increase from 30 to 130 nm, as the power confinement in the Si core increases, so power in GSST layer reduces. The waveguide with thicker GSST thickness T suffers from higher mode loss compare to others. On the other hand, the mode loss for the crystalline state also decrease but more slowly with S , and it also shows that for larger T , waveguide suffers from a higher modal loss. It can be concluded that a thinner GSST layer can yield smaller modal loss values and waveguide with a larger slab thickness can also achieve slightly lower modal loss for both the states.

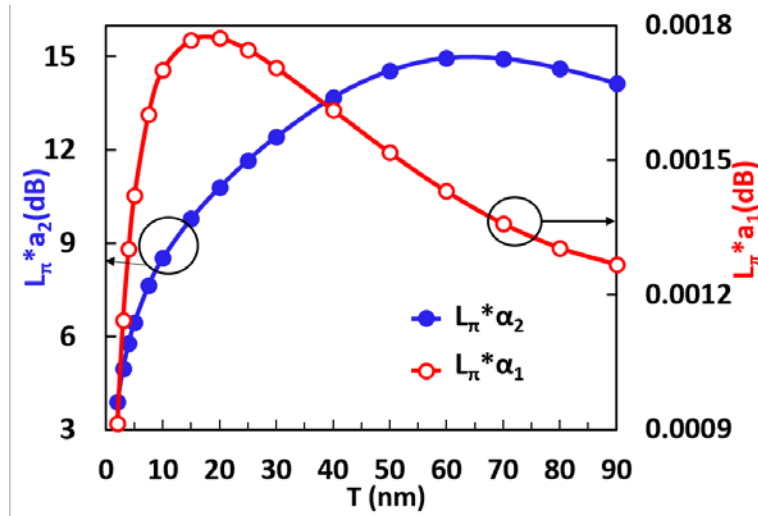


Fig. 6. Total modal loss of CW in amorphous and crystalline states with varying GSST thickness T .

Variations of the total modal loss ($L_{\pi} * \alpha_1$) of CW with the GSST thickness, T , for MZI based device of length $= L_{\pi}$, with $W = 500$ nm and $S = 90$ nm for the amorphous state is shown by a red line in Fig. 6. When the GSST thickness T increases from 2 to 15 nm, the total loss value increase quickly from 0.0009 to 0.0018 dB. After that, the total modal loss decrease slightly from 0.0018 to 0.0013 dB as the T increases to 90 nm as the device length reduces more rapidly. On the other hand, the total modal loss for the crystalline state ($L_{\pi} * \alpha_2$) shown by a blue line increases from 4 to 15 dB with the T increase from 2 nm to 60 nm then it decreases a little bit around 14 dB with the T between 60-90 nm. These values are much higher than those for the amorphous state.

Although, a small 4-7 dB total modal loss of CW in crystalline state when the GSST thickness T is between 2 to 10 nm may allow a possible MZI switch, however device length needs to be longer than 20 μ m which may be less attractive for a compact MZI design. On the other hand, when the T increase to a higher value, L_{π} reduces, which although may yield a compact switch, but the resulting 10-15 dB modal loss for the crystalline states will cause a poor switching extinction ratio due to incomplete field cancellation.

It is clear from the previous results that the ER based approach may not be suitable for a possible GSST switch, so next the EA ($k_{e2}-k_{e1}$) effect will be used for the possible switch design.

Here, it is assumed that the switch will need a total extinction ratio of 20 dB between amorphous and crystalline states. If desired, any other preferred extinction ratio can also be considered. In this particular case, the corresponding device length L_{20dB} can be calculated as:

$$L_{20dB}(\mu\text{m}) = \frac{20}{(\Delta\alpha)} = \frac{20 \text{ dB}}{(\alpha_2 - \alpha_1) \text{ dB}/\mu\text{m}} \quad (6)$$

If we consider a GSST CW section of length L_{20dB} is considered, then the modal loss for the crystalline state would be 20 dB higher than that of the amorphous state.

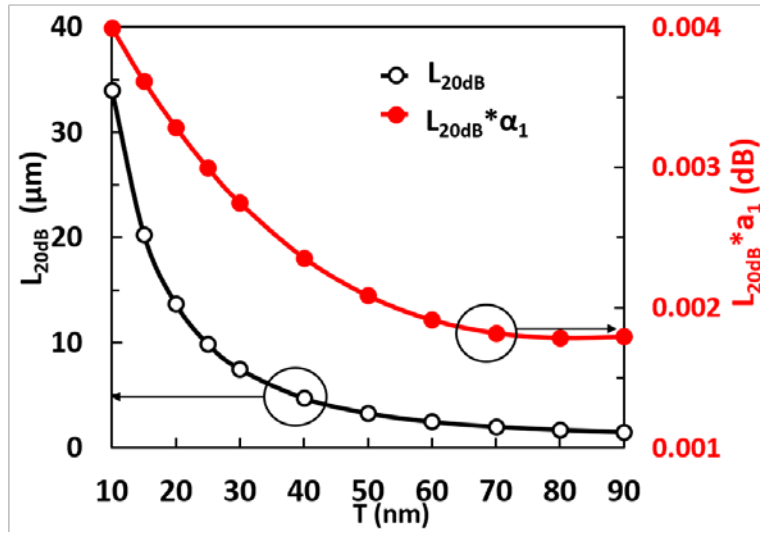


Fig. 7. L_{20dB} and total modal loss of CW in amorphous state with varying GSST thickness, T.

When the $W = 500 \text{ nm}$ and $S = 90 \text{ nm}$, variations of switch length, L_{20dB} and total modal loss of the amorphous state ($L_{20dB} * \alpha_1$) with the GSST thickness, T are shown in Fig. 7. The switch length L_{20dB} is shown by a black line with hollow circles. When the T increases from 10 to 40 nm, the L_{20dB} decreases monotonically from 35 μm to a lower 5 μm . When the T increases further to 90 nm, the switch length L_{20dB} decreases slowly to 1.54 μm , which shows that a compact optical switch is viable. Total modal loss of the switch for a low-loss “ON” state is shown by a red line with solid circles using the right-hand side scale. It can be noticed that the total modal loss of the amorphous state reduces from 0.004 dB to 0.0018 dB when T increases from 10 nm to 90 nm. It can be concluded here, a higher GSST thickness T, around 40-90 nm can yield a switch shorter than 5 μm , and the total modal loss for “ON” state would be very low around 0.0018 dB.

It also can be noted that when $T = 20 \text{ nm}$, the L_{20dB} increases monotonically from 11.5 to 16 μm when the S increase from 30 to 130 nm, but not shown here. However, when $T = 60$ and 90 nm, their switch lengths increase very slowly from around 1.8 to 2.2 μm when S increase from 30 nm to 130 nm. On the other hand, it can also be noted that when $T = 20 \text{ nm}$, the modal loss reduces slowly from 0.0034 to 0.0032 dB when the S increase from 30 to 130 nm. Similarity, when $T = 60$ and 90 nm, their modal loss values also decrease slowly from around 0.0021 to 0.0016 dB when S increase from 30 nm to 130 nm. It can be concluded that when a 60-90 nm GSST layer is loaded on the Si rib waveguide, the larger Si slab thickness S can achieve a short device length around 2 μm and a lower modal loss only 0.0016 dB for the “ON” state.

The modal field profiles for the active CW at amorphous and crystalline states were shown in Fig. 2. These field profiles were different due to the significant changes in the GSST refractive index when GSST phase changes. This suggests the possibility of a considerable power loss at junction 1 and 2 due to the mismatch between the modes field profiles at these junctions.

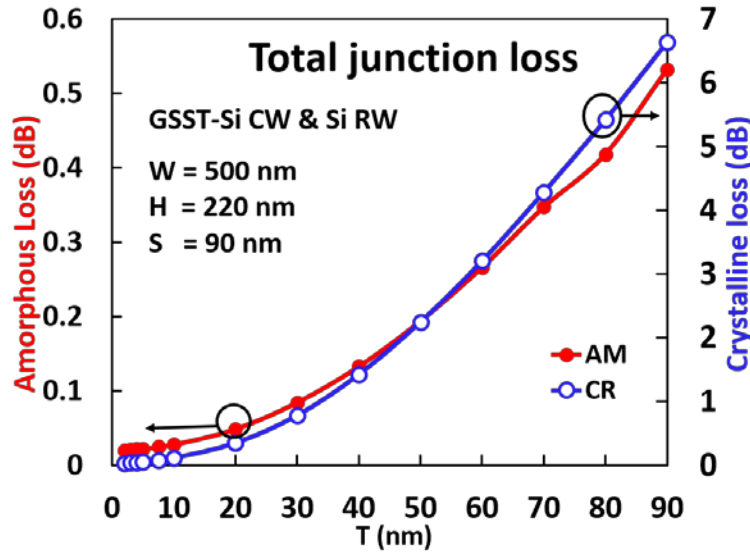


Fig. 8. Variation of the total junction loss of CW in amorphous and crystalline states with the GSST thickness, T.

The effect of GSST layer thickness T on the junction loss is studied. In this case, for S = 90 nm, the total junction losses of active CW from coupling to passive RW at both input and output sides, calculated by the LSBR method for the amorphous state, are shown by a red line in Fig. 8. It shows that when the slab thickness T increases from 2 to 90 nm, the total junction loss increases from a lowest value of 0.02 dB to 0.53 dB. Total junction loss of CW in crystalline state is also shown by a blue line using the right-hand side scale. In this case, the junction loss increases exponentially from 0.03 dB to 6.64 dB when the T increases from 2 nm to 90 nm. Junction loss for crystalline state is significantly higher as higher index value with thicker GSST layer make the modal field very different than that of the unclad RW.

Here, it can be concluded that smaller GSST thickness T can yield a satisfactory design with a lower junction loss at the amorphous “ON” state, however it will require a much longer device length, so the optimized GSST thickness need to be selected to balance both of these parameters. On the other hand, the additional coupling loss in the crystalline state not that critical as being related to the “OFF” state.

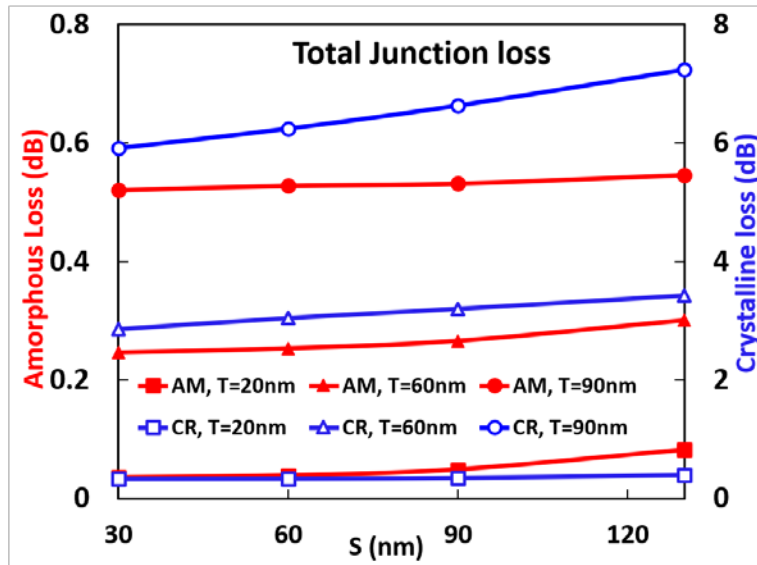


Fig. 9. Variation of the total junction loss of CW in amorphous and crystalline states with the slab thickness, S for different GSST thickness T.

Next, effect of Si slab thickness S of the total junction loss is also calculated. For $T = 20, 60$ or 90 nm, the total junction loss for these two states from both the junctions as a function of the slab thickness, S are shown in Fig. 9. Results for the amorphous state are shown by red lines, using the left-hand side scale, and it can be observed that, the total junction loss of the waveguides with different GSST thickness, T increase slightly with the Si slab thickness, S. A thinner 20 nm GSST layer can yield lower junction loss, only 0.035 dB, but even for 90 nm thick GSST layer could suffer only 0.53 dB, which still acceptable for the switch design. Total junctions for the crystalline state are shown by blue lines using the right-hand side scale, which increases slowly with S, and it also shows that for larger T, waveguide can incur a higher junction loss. It can be concluded that a thinner GSST layer can provide smaller junction loss and additionally a smaller slab thickness waveguide can also achieve lower total junction loss for both the states.

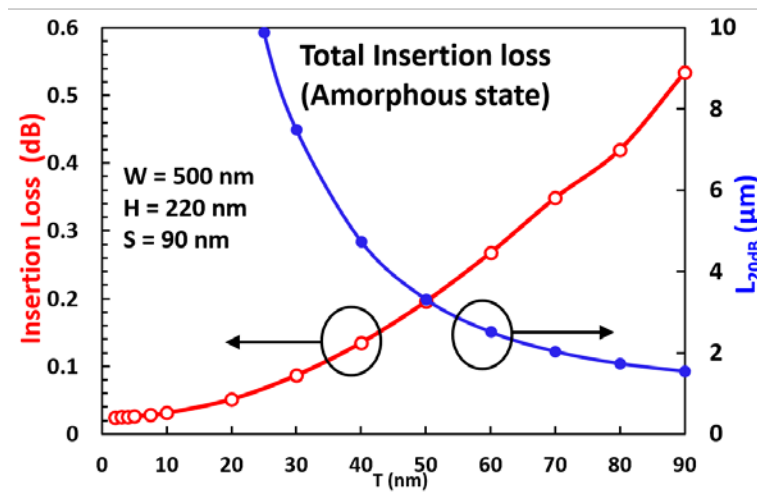


Fig. 10. Variations of total insertion loss and L_{20dB} of CW in amorphous state with GSST thickness T.

The associated lower insertion loss suggests that a viable optical switch at the “ON” state can be obtained when GSST is in amorphous state. The total loss is comprised of the modal loss of the active GSST CW section due to the absorption in the GSST cap and the coupling loss between the passive input and output Si RW sections and the active GSST CW section.

From Figs. 8 and 9, it was observed that the total junction loss is the dominant factor of the total insertion loss as the total modal loss has been lower than 0.005 dB for the whole range of T considered here. Here, for $S = 90$ nm, the associated total Insertion Loss of GSST CW is shown by a red line in Fig. 10. It can be observed that, when GSST thickness T increases from 2 to 10 nm, the total insertion loss of the switch increases slightly from a relatively low value 0.025 to 0.03 dB. After $T=10$ nm, the total insertion loss increases exponentially from 0.03 to 0.53 dB with the GSST thickness T increase to 90 nm. The required device length, L_{20dB} is shown again in this figure.

If a compact switch with length shorter than $5 \mu\text{m}$ is preferred, then the GSST thickness T should be larger than 40 nm to achieve it. From Fig. 10, it can be concluded that the 40-60 nm thicker GSST layer may be a preferred design, which shows a small total insertion loss value of 0.13-0.27 dB, also yielding a compact device with length between 2.5 and $5.0 \mu\text{m}$.

On the other hand, the insertion loss variation of the amorphous state with the Si thickness, S is fairly constant but not shown here. It can be noted that as the total insertion loss increase very slowly with the Si slab thickness, and when the $S = 60-90$ nm, the total insertion loss has the smallest change, and this can be taken as an optimal design for the GSST CW. The switch is designed and optimized to show a 20 dB higher modal loss in the crystalline state compared to the amorphous state. Additionally, the crystalline state has higher junction loss shows than the amorphous state. Therefore, the total insertion loss in the ‘OFF’ state (crystalline) exceeding 20 dB compared to the ‘ON’ state (amorphous).

Table. 2 Performance comparison between GST and GSST design.

PCM	PCM thickness (nm)	Device length (μm)	Min IL (dB)
GST	25	2.27	0.359
GSST	40	4.75	0.135
	50	3.32	0.196
	60	2.51	0.268

We have recently reported a GST-clad Si waveguide based optical switch design with $2.27 \mu\text{m}$ device length and a minimum insertion loss 0.359 dB and this is given in Table. 2 [14]. However, if low-loss GSST used in the EA switch design, the minimum insertion loss could be reduced to only 0.135 dB, which is 38% of the earlier GST based design and with a $4.75 \mu\text{m}$ device length shows a greater potential for low loss PICs. On the other hand, a more compact device with slightly thicker GSST layer, say 60 nm can also be attractive with the total insertion loss still smaller than the GST based designs.

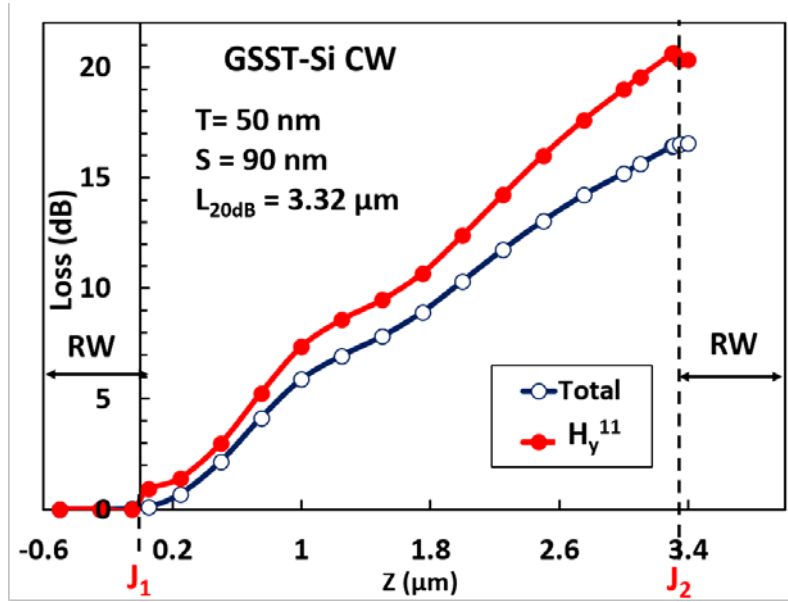


Fig. 11. Variations of total insertion loss and fundamental mode insertion loss of switch when GSST in crystalline state with $T = 15$ nm, $S = 90$ nm and $L_{20\text{dB}} = 3.32$ μm by FDTD simulation.

To validate these results, we have also simulated the complete optical switch with $S = 90$ nm, $T = 50$ nm and $L_{20\text{dB}} = 3.32$ μm using the 3D Lumerical FDTD package and shown in Fig. 11. A non-uniform mesh distribution has been considered for the FDTD computations with a mesh accuracy of 7. An extra mesh size of ($dy = 5$ nm, $dz = 5$ nm) for the thin GSST layer is added for the better accuracy. Here, evolution of power of the fundamental H_y^{11} mode along the propagation direction Z is shown by a red line. At Junction 1, $Z = 0$ μm , there is about 1 dB optical loss, which agree with the LSBR simulations. The power loss monotonically increases until $Z = 3.32$ μm , at junction 2. Here, total power loss of the H_y^{11} mode when GSST in crystalline state is more than 20 dB which agrees to our full-vectorial FEM modal solution. Small ripple is likely due to the periodic interference between the propagating modes.

At these junctions, higher order modes are generated to satisfy the boundary conditions. So next, evolution of total power is obtained. The total optical power, comprising the H_y^{11} and higher order modes along the propagation direction Z is shown by a blue line in Fig. 11. It is noticeable that the total optical loss increases to 16.5 dB at the junction 2. The overall optical power loss of the switch was less than 20 dB due to generation of higher order modes at junction 1 followed by recombination of some of them at junction 2. If a 20 dB extinction ratio is required for total power (rather than the fundamental modal loss), then the length of the device need to be increased slightly.

4. CONCLUSION

A rigorous modal analysis of a self-sustained switch based on a GSST-Si rib waveguide at the wavelength 1.55 μm is conducted by using an accurate \mathbf{H} -field based full-vectorial FEM and benchmarked by using FDTD method. It was observed that although GSST layer can yield a high ER values, however due to the associated higher mode loss in crystalline state, a conventional MZI switch design will not be viable. Therefore, exploiting the large modal loss between the GSST amorphous and crystalline states, an EA-type switch design is more

effective. In this report, the device performance is enhanced by optimizing the GSST-layer thickness (T) and Si slab thickness (S).

It is observed that a GSST thickness over 40 nm yields a much preferable compact device length $>5 \mu\text{m}$ with a lower modal loss. A 2 to 90 nm GSST variation in the amorphous state introduces a total modal loss lower than 0.005 dB. Besides, the mode mismatch with the GSST thickness variation incorporates an additional junctional loss which is a dominating fraction in the total insertion loss. It is noticeable that a satisfactory low junctional loss from 0.132 to 0.266 dB can be achieved with a 40 – 60 nm GSST thickness, also considered as an optimal GSST thickness (T) to balance the device length with low insertion loss.

Moreover, the insertion loss slowly varied with the dielectric Si slab thickness. A 60 – 90 nm Si slab thickness is considered as an optimal design for the Si rib waveguide due to its smallest insertion loss changes in this region. Considering the full structure, the Si-GSST rib waveguide is advantageous over fully etched Si nanowire as it introduces an additional scattering loss at the sidewalls and edges.

In summary, a GSST-Si rib waveguide with optimized design parameters, such as width, $W = 500 \text{ nm}$, slab thickness, $S = 60\text{-}90 \text{ nm}$, and GSST thickness, $T = 40\text{-}60 \text{ nm}$ works as a self-sustained switch. An extinction ratio more than 20 dB between ‘OFF’ and ‘ON’ states is achieved with a small insertion loss of 0.135 dB at the ‘ON’ state. Additionally, it is observed by the FDTD simulations, that power loss of the fundamental H_y^{11} mode was more than 20 dB, however total optical loss was 16 dB due to generation and reconversion of higher order modes.

REFERENCES

1. G. T. Reed, G. Mashanovich, F. Y. Gardes and D. J. Thomson, "Silicon optical modulators", *Nature Photon*, vol. 4, pp. 518-526, 2010.
2. M. Wuttig, H. Bhaskaran, and T. Taubner, "Phase-change materials for non-volatile photonic applications," *Nature Photon*, vol. 11, no. 8, pp. 465-476, 2017.
3. A. Joushaghani, J. Jeong, S. Paradis, D. Alain, J. S. Aitchison, and J. K. Poon, "Wavelength-size hybrid Si-VO₂ waveguide electroabsorption optical switches and photodetectors," *Opt. Express*, vol. 23, no. 3, pp. 3657-68, 2015.
4. D. Tanaka, Y. Shoji, M. Kuwahara, X. Wang, K. Kintaka, H. Kawashima, T. Toyosaki, Y. Ikuma, H. Tsuda, "Ultra-small, self-holding, optical gate switch using Ge₂Sb₂Te₅ with a multi-mode Si waveguide," *Opt. Express*, 20(9), 10283-10294 (2012).
5. H. Liang, R. Soref, J. Mu, A. Majumdar, X. Li, and W. Huang, "Simulations of silicon-on-insulator channel-waveguide electro-optical 2 x 2 switches and 1 x 1 modulators using a Ge₂Sb₂Te₅ self-holding layer," *J. Lightw. Technol.*, 33(9), 1805-1813 (2015).
6. M. Stegmaier, C. Rios, H. Bhaskaran, and W. H. P. Pernice, "Thermo-optical effect in phase-change nanophotonics," *ACS Photonics*, vol. 3, no. 5, pp.828-835, 2016.
7. T. Moriyama, H. Kawashima, M. Kuwahara, X. Wang, H. Asakura, and H. Tsuda, "Small-sized Mach-Zehnder interferometer optical switch using thin film Ge₂Sb₂Te₅ phase-change material," *Optical Fiber Communications Conference and Exhibition, San Francisco, USA, 2014*, p. Tu3E.4.
8. K. Kato, M. Kuwahara, H. Kawashima, T. Tsuruoka, and H. Tsuda, "Current-driven phase-change optical gate switch using indium-tin-oxide heater", *Appl. Phys. Express*, vol. 10, no. 7, p. 072201, 2017.
9. H. Zhang, L. Zhou, B. M. A. Rahman, X. Wu, L. Lu, Y. XU, J and J. Song "Ultracompact Si-GST hybrid waveguides for nonvolatile light wave manipulation," *IEEE Photonics Journal*, Vol. 10, Issue 1, Feb. 2018.
10. Q. Zhang, Y. Zhang, J. Li, R. Soref, T. Gu, and J. Hu, " Broadband nonvolatile photonic switching based on optical phase change materials: beyond the classical figure-of-merit," *Optics Letters*. Vol. 43, Issue 1, pp. 94-97 (2018)
11. B. M. A. Rahman and J. B. Davies, "Finite element solution of integrated optical waveguides," *J. Lightw. Technol.*, Vol. 2, no. 5, pp. 682–688, 1984.
12. C. Themistos, B. M. A. Rahman, A. Hadjicharalambous, and K. T. V. Grattan, "Loss/gain characterization of optical waveguides," *J. Lightw. Technol.*, Vol. 13, no. 1, pp. 1760–1765, Aug. 1995.
13. B. M. A. Rahman and J. B. Davies, "Analyses of optical waveguide discontinuities," *J. Lightw. Technol.*, Vol. 6, no. 1, pp. 52–57, Jan. 1988.
14. J. Song, S. Ghosh, N. Dhingra, H. Zhang, L. Zhou, and B. M. A. Rahman, "Feasibility study of a Ge₂Sb₂Te₅-clad silicon waveguide as a non-volatile optical on-off switch," *OSA Continuum*, Vol. 2, Issue 1, pp. 49-63 (2019)
15. Lumerical FDTD Solution. Available online: <http://www.lumerical.com>